Proceedings of CONF-MSS 2026 Syposium: Mechanical Control and Automation
DOI: 10.54254/2755-2721/2026.BJ32898

3D Perception Network: An Integrated Multi-Parameter Monitoring Platform for Mulberry Fish Ponds

Jiayao Shen

Hertfordshire College, Changzhou Institute of Technology, Changzhou, China
24260522@czu.cn

Abstract. As a typical sustainable agricultural model in the water network areas of southern China, mulberry fish ponds promote the coordinated development of sericulture, silkworm rearing and fish farming. This study developed an amphibious unmanned aerial vehicle (UAV)-mounted multi-parameter monitoring platform for mulberry fish ponds. It features a wheel-track and paddle wheel composite drive for seamless land-water transition, and a non-magnetically constrained high-seal transmission for reliable operation in humid environments. Its water-soil-air multi-sensor system enables comprehensive environmental perception, while the multispectral camera-equipped UAV realizes early disease identification via ground-air collaboration. Field tests show land and water speeds of 1.01 m/s and 0.48 m/s respectively, with monitoring error ≤3%. It improves operational efficiency by 5-8 times over manual methods, achieves over 95% disease detection accuracy, cuts total energy consumption by more than 30%, and extends UAV operation time by 40%. This system provides an innovative technical solution for the intelligent transformation of traditional ecological agriculture.

Keywords: mulberry fish pond, amphibious, multi-parameter monitoring, smart agriculture

1. Introduction

The "Asia and the Pacific SDG Progress Report 2026" released by the United Nations Economic and Social Commission for Asia and the Pacific (ESCAP) stresses the continued need for sustainable development [1]. Mulberry fish ponds are a representative ecological farming system in southern China's water-network region [2,3]. They connect mulberry cultivation, silkworm rearing, and fish farming within one cycle. Valuable system. Yet management is still labor-intensive. Disease outbreaks in mulberry trees cannot always be found early, and the alternating pattern of pond water and narrow ridges makes routine inspection slow and uneven. Real-time, amphibious monitoring equipment is therefore needed.

Amphibious robots are commonly divided into bionic types and wheel-track types [4-7]. Bionic designs are flexible, but engineering tasks usually favor wheel-track structures because they carry more load and move more steadily on land. The problem is that many existing systems still struggle in mixed land-water environments: switching mechanisms are bulky, sealing is weak, and energy use rises sharply in soft terrain. Earlier studies examined drag reduction in sectional crawler vehicles and wheel-leg structures for complex terrain [8-10]. Building on that work, this study follows a four-

© 2026 The Authors. This is an open access article distributed under the terms of the Creative Commons Attribution License 4.0 (https://creativecommons.org/licenses/by/4.0/).

DOI: 10.54254/2755-2721/2026.BJ32898

step route—analysis, design, prototype fabrication, and testing—to develop an amphibious-aerial collaborative platform for monitoring, disease warning, and ecological management in mulberry fish ponds.

2. System design and technical principles

2.1. Overall structure and modular layout

The platform uses a modular layout with six units: drive, information acquisition, UAV, control, buoyancy compensation, and path planning. Overall dimensions are 800 mm × 597.68 mm × 516.75 mm. Fiberglass board is selected as the main structural material to keep the body light while maintaining strength and corrosion resistance, which matters on narrow pond ridges. The water-quality sensor is mounted beneath the vehicle so it can remain fully submerged in water while still keeping 70 mm of ground clearance on land. The soil sensor is linked to a vertical electric pushrod with 119 mm of lifting travel and a maximum insertion depth of 71 mm. The air sensor is fixed on the top surface, and the UAV module is attached to the upper platform through electromagnetic adsorption. Layered layout. Better balance, easier sensing, easier maintenance.

2.2. Amphibious composite drive mechanism

2.2.1. Wheel-track-paddle wheel composite drive principle

Mulberry fish ponds force the vehicle to cross narrow ridges, shallow water, and muddy transition zones in quick succession, so the platform adopts a wheel-track-paddle-wheel composite drive that lets one power source handle both travel modes without a separate switching unit. On land, the tracks provide differential motion for travel and steering. On water, the paddle wheels take over. Simple. This arrangement keeps the mechanism compact and links the motor, paddle wheels, tracks, and rollers in one transmission chain. In tests, the platform reached 1.01 m/s on land and 0.48 m/s on water. It stayed stable during land-water transition.

2.2.2. Non-magnetically constrained high-sealability transmission design

Many amphibious robots still depend on magnetically constrained transmission structures, but those layouts eat up internal space, cap torque, and make sealing harder. So we took another route. The platform uses an integrated mechanical transmission made up of the motor, output shaft, plates, connectors, waterproof bearings, and couplings. The custom connector locks the waterproof bearing to the load-bearing plate, and the motor shaft presses into the bearing inner race through a high-precision interference fit. The idea is simple: compress the interface radially, remove the gap, and block water ingress. Tests in humid conditions and short-term immersion showed no water leakage, obvious lag, or corrosion. Reliable enough for field use.

2.2.3. Power system matching

The power system consists of a 24 V/20 Ah lithium battery pack and a 17.05 N·m brushless DC motor. Mechanical analysis shows that the maximum rolling-friction torque of the driven wheel can reach 27 N·m on muddy ground. After transmission conversion, the motor still keeps a sufficient torque margin. Under a typical 30°slope, the total resistance torque of the driving wheel is only

DOI: 10.54254/2755-2721/2026.BJ32898

1.229 N·m, giving a reserve of more than 13 times. That reserve supports the 45° extreme design slope used in later tests.

2.3. Buoyancy regulation and waterproof sealing system

2.3.1. Adaptive buoyancy regulation mechanism

The buoyancy-regulation subsystem uses a high-torque servo motor, a reduction mechanism, and a synchronous belt. Closed-loop angle control lets the system shift float position with good accuracy and keep buoyancy compensation stable. Once the vehicle enters water, the floats swing down and extend, which raises displacement; once it climbs back onto land, they retract and free up space. Compact again. Calculations give a total displacement volume of about 348,480 mm^3, which translates into nearly 90 N of buoyancy and offsets most of the vehicle weight. The predicted draft is 193.4 mm. Still below the 200 mm target.

2.3.2. Mechanical sealing technology

The transmission section bears most of the sealing pressure, so we treated it as a mechanical problem rather than a packaging detail. The platform relies on an interference-fit seal created by radial compression between the motor output shaft and the inner race of the waterproof bearing. Tight fit. This layout blocks the main route for moisture intrusion, avoids the torque ceiling seen in magnetic-drive sealing, and keeps the structure easier to build. Humid-air tests and short immersion tests showed that the seal kept working. Figure 1a gives the physical prototype, and Figure 1b gives the 3D model.



Figure 1. Physical prototype of the monitoring platform

(a) Physical photo of monitoring equipment (b) 3D model diagram of monitoring equipment

3. Multi-parameter perception and intelligent decision-making

3.1. Integration of water, soil and air multi-source sensors

3.1.1. Configuration of sensor units

To monitor the mulberry fish pond ecosystem from several dimensions, the platform integrates water-quality, soil, and air sensors. The water-quality unit is a PTH-800-13 multi-parameter sensor that measures water temperature, pH, dissolved oxygen, electrical conductivity, and turbidity. The target accuracy is ±0.1 mg/L for dissolved oxygen and ±0.1 for pH. Soil data are collected with the PTH-700-21 isolated sensor, which uses ion-selective electrode technology to measure soil

DOI: 10.54254/2755-2721/2026.BJ32898

temperature, volumetric water content, salinity, and the contents of nitrogen, phosphorus, and potassium; its nutrient sensitivity is 1 mg/kg. The air unit is a PTH-700-01 louver sensor for air temperature, humidity, pressure, light intensity, and noise. Enough to cover the basic environmental state.

3.1.2. Sensor layout and sampling strategy

Sensor placement follows measurement needs and vehicle motion, not a neat geometric pattern. The water-quality sensor sits under the vehicle with 70 mm of ground clearance, so it stays fully submerged after the platform enters water. The soil sensor rides on a vertical electric pushrod with a 119 mm stroke and a maximum insertion depth of 71 mm, and its probe diameter is 5 mm. The air sensor stays on top. Different spots. For data collection, the system mixes periodic polling with event triggering. Under normal conditions, it samples at fixed intervals; when parameters change sharply or the vehicle reaches a key area, it immediately raises the sampling frequency. The main controller receives every sensor signal through the CAN bus and processes them in sync.

3.2. Ground-air collaborative three-dimensional perception architecture

3.2.1. Path planning for the ground platform

The ground platform plans its path with a hybrid method that combines an improved A* algorithm with the dynamic window approach, because ridges in mulberry fish ponds do not forgive slow decisions. An Intel RealSense depth camera gathers 3D point-cloud data ahead of the vehicle and gives the controller richer spatial cues than 2D vision. More detail. The improved A* stage adds terrain cost to global planning, so the vehicle chooses routes with lower energy demand and better traversability. The dynamic window approach handles local obstacle avoidance, while GPS and odometer data support path tracking. In tests, planning response stayed within 100 ms, and the vehicle moved on muddy ridges and slopes up to 45° autonomously.

3.2.2. Disease identification using UAV

The UAV carries a high-definition industrial camera and a multispectral imager so it can inspect the mulberry canopy before disease spreads far. We built disease recognition on YOLOv5 and trained it with more than 2,000 annotated images of leaves affected by bacterial blight and brown spot. Enough data. Data augmentation helps when lighting or leaf posture changes. The workflow covers route planning, image capture, spectral-feature extraction, and diagnosis. The multispectral module also records near-infrared information, which lets the system catch anomalies before symptoms become obvious. Tests gave recognition accuracy above 95% and positioning accuracy of about ±0.5 cm.

3.2.3. Vehicle-uav collaborative operation mode

The system splits work between the ground platform and the UAV so it can cover more area without burning through power too fast. The vehicle handles routine inspection, gathers multi-parameter data, and moves along ridges or across water; the UAV steps in when canopy inspection becomes necessary or when the vehicle reaches a narrow section. Clear division. The system selects a release position and sends out the UAV through an electromagnetic adsorption mechanism. After a short scan, the UAV returns for landing and charging on the platform. This arrangement extends effective

DOI: 10.54254/2755-2721/2026.BJ32898

UAV working time by 40% and cuts total energy consumption by more than 30% compared with conventional methods.

3.3. Data fusion and intelligent warning

3.3.1. Adaptive weighted fusion of multi-source data

Water, soil, and air data arrive on different time scales and carry different physical dimensions, so the platform does not mix them with a fixed rule. It uses an adaptive weighted fusion algorithm. Step by step. The system removes outliers and normalizes raw signals, then assigns fusion weights according to sensor confidence and updates that confidence with real-time variance and historical accuracy. The fused results stay steadier. For instance, the system can read turbidity together with nitrogen and phosphorus content to infer shifts in organic matter and guide nutrient management.

3.3.2. Real-time decision-making closed loop based on edge computing

A Jetson NX platform handles data preprocessing, model inference, and decision generation on the vehicle, which keeps key tasks close to the sensors. The edge-side lightweight neural network predicts short-term trends in soil nutrients and water-quality indicators. Fast response. When any parameter crosses its threshold, the system sends a local warning and uploads the data to the cloud. The edge node handles millisecond-level reactions, while the cloud stores long-term records and supports cross-region comparison. That split lowers network dependence and still keeps real-time control.

3.3.3. Multi-level warning mechanism and remote transmission

The warning subsystem works in three levels. Level 1 shows an informative warning on the vehicle. Level 2 pushes an alert to the mobile app through the ESP8266 module. Level 3 goes further. It triggers protective actions such as vehicle shutdown or float deployment and uploads data to Alibaba Cloud through the 4G network. The system sends messages with MQTT and keeps the transmission delay within 1 s. When the network drops, local caching and automatic retransmission keep the records from disappearing. The database stores every warning for later analysis and model adjustment.

4. Performance testing and result analysis

4.1. Dynamic performance of the mobile platform

Land-motion performance was evaluated through theoretical calculation and experiment. The total vehicle mass is m = 9 kg, so the weight is G = mg = 88.2 N. Because the platform uses a tracked drive, rolling resistance on the driven wheel must be considered when estimating translational performance.

$$M=fG \tag{1}$$

The rolling-resistance factor f varies with ground condition. Under the harshest muddy-road case, f = 0.3 m is used. On that basis, the maximum rolling-friction torque on the driven wheel is obtained

DOI: 10.54254/2755-2721/2026.BJ32898

as follows:

$$M_1 = f_{max}\,\mathrm{G} = 0.3 \times 88.2 = 26.46\ \mathrm{N{\cdot}m} \tag{2}$$

After transmission efficiency is considered, the equivalent resistance torque that the driving wheel must overcome can be derived from the torque-balance relation:

$$M_2 = \frac{M_1 R}{L} \tag{3}$$

With driving-wheel radius R = 17 mm and track-ground contact length L = 600 mm, the calculated resistance torque is M2 ≈ 0.75 N·m. The rated motor torque is M3 = 17.05 N·m, much larger than M2, which confirms that the drive system can overcome rolling resistance on land.

Using the rated motor speed n1 = 560 r/min and the driving-wheel radius R, the theoretical translational speed is:

$$V_1 = 2\pi n_1 \mathrm{R} = 2\pi \times \frac{560}{60} \times 0.017 \approx 1.00 \mathrm{m/s} \tag{4}$$

The measured average land speed is 1.01 m/s, in good agreement with the theoretical value.

Climbing ability was also analyzed for the slopes commonly found in mulberry fish ponds. A slope angle of θ = 30° was taken as the representative working condition. Under this case, the gravitational-resistance torque and rolling-resistance torque acting on the driving wheel are expressed as:

$$M_5 = \mathrm{GR}\sin\theta = 0.750 \mathrm{N{\bullet}m} \tag{5}$$

$$\mathrm{M_6} = \mathrm{G}f_1\mathrm{R}\cos\theta = 0.065 \mathrm{N{\bullet}m} \tag{6}$$

Accordingly, the total resistance torque can be written as:

$$M_7 = M_6 + M_5 = 0.815 N{\bullet}\mathrm{m} \tag{7}$$

The rated motor torque is about 17.05/0.815 ≈ 20.9 times the total resistance torque. Put simply, the power reserve is ample. Field tests confirmed stable operation on muddy roads and on slopes up to 45°.

DOI: 10.54254/2755-2721/2026.BJ32898

4.2. Verification of multi-parameter monitoring accuracy

4.2.1. Calibration experiment of water quality sensor

The water-quality sensor was calibrated with standard solutions and field water samples. pH, dissolved oxygen, electrical conductivity, and turbidity were monitored continuously. During testing, pH stayed between 6.8 and 7.2 and dissolved oxygen ranged from 5.2 to 6.8 mg/L. Compared with laboratory reference instruments, the error of each parameter remained below 3%, meeting the design target. Sensor response time was also adequate for real-time use.

4.2.2. Calibration experiment of soil sensor

The soil sensor was tested in soils with different textures and moisture levels. It recorded soil temperature, volumetric water content, and nitrogen, phosphorus, and potassium content. The measured nitrogen values showed a clear linear relation with the actual fertilizer input, which supports the sensor's reliability for nutrient monitoring. The probe reached an insertion depth of 71 mm and worked normally under different soil conditions.

4.2.3. Calibration experiment of air sensor

The air sensor continuously recorded temperature, humidity, and light intensity under changing outdoor conditions. The results matched the expected daily variation of these factors. The temperature error did not exceed ±0.5°C, and the light-intensity range of 0–200 klux covered the needs of mulberry growth monitoring. Humidity response also met the design specification.

4.3. Field comprehensive tests and optimization

4.3.1. Water-land transition and ground-air collaborative operation test

Field experiments were conducted at a site simulating the mulberry fish pond environment. During land-water transition tests, the platform moved from land to water and back again without jamming or overturning. The adaptive floats deployed automatically in water and retracted after landing. UAV trials further verified the ground-air collaborative mode: takeoff and landing through the electromagnetic release mechanism were smooth, hovering accuracy reached ±0.5 cm, and the collected images satisfied the requirement for disease identification. Figure 2 shows the prototype in water, Figure 3 shows UAV flight, and Figure 4 shows land driving.

DOI: 10.54254/2755-2721/2026.BJ32898

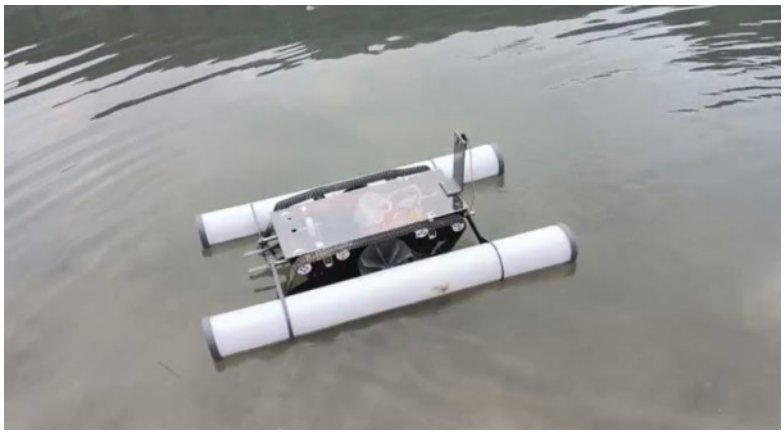

Figure 2. Inter-tank test



Figure 3. UAV flight test

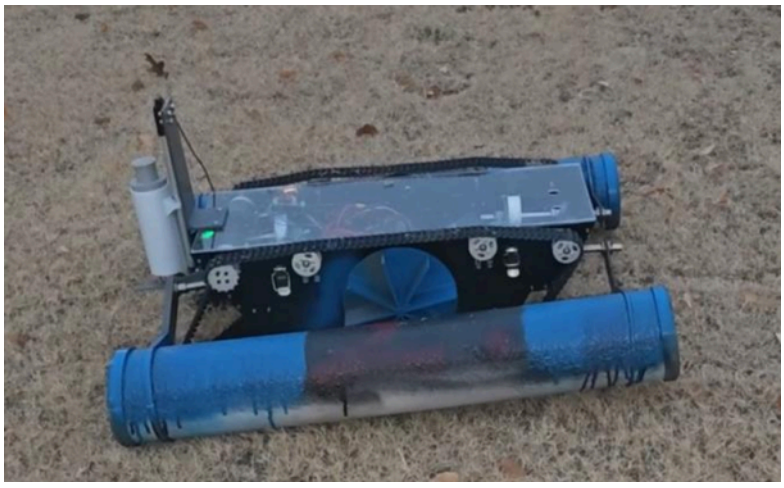

Figure 4. Ridge test

DOI: 10.54254/2755-2721/2026.BJ32898

4.3.2. Comparison of operation efficiency and energy consumption analysis

Platform efficiency was compared with manual monitoring. For tasks covering multiple pond areas, the system completed full-area monitoring in roughly one-fifth to one-eighth of the time required by human operators, which corresponds to a 5–8-fold improvement. Energy use also decreased. The paddle-wheel-track drive and the scheduling strategy reduced total system energy consumption by more than 30%, while effective UAV operating time increased by 40%.

4.3.3. Existing problems and improvement directions

Field tests also exposed several issues. Water-navigation speed was lower than the design target, so paddle-wheel geometry and drive parameters still need optimization. Sharp-turn stability was not ideal. The next version is planned to include a servo-driven suspended float system for adaptive buoyancy adjustment after water entry, together with reversible thrusters at the front and rear to improve maneuverability and emergency braking in water. Those changes should reduce collision risk, though full verification still requires longer field trials.

5. Conclusion

This paper presented an amphibious UAV-mounted multi-parameter monitoring platform for mulberry fish ponds. The system combines wheel-track motion, paddle-wheel propulsion, high-seal mechanical transmission, and a water-soil-air sensing architecture, while also supporting UAV-based disease detection. Tests showed stable travel on land, in water, and on 45° pond ridges. Monitoring error remained within 3%, operating efficiency increased by 5–8 times over manual methods, and disease-recognition accuracy exceeded 95%. Total energy use was reduced by more than 30%, and UAV effective working time increased by 40%. The study mainly verified the prototype and its basic field performance. Long-term reliability, sensor drift, and seasonal robustness still need more evidence. Whether the platform can be extended efficiently to other integrated farming systems—such as rice-fish agriculture—remains an open question.

References

[1] United Nations Economic and Social Commission for Asia and the Pacific. Asia and the Pacific SDG Progress Report 2026 [R/OL]. (2026-02-18) [2026-03-08]. https: //www.unescap.org/kp/2026/asia-and-pacific-sdg-progress-report-2026.
[2] Pan Y. Application and Innovative Path of the Mulberry-Dyke and Fish-Pond Ecological Circulation Model in Landscape Design [J]. China Fishing, 2025(01): 71-73.
[3] Ma W Y, Xu Y M, Wang Y J. Path Planning of Amphibious Robot Based on Improved Artificial Potential Field Method [J]. Modular Machine Tool & Automatic Manufacturing Technique, 2022(12): 10-13+17.
[4] Zhang J, Zhou J J, Yuan S H, et al. Review on Configuration, Motion Mechanism and Modeling Control of Amphibious Bionic Robots [J]. Robot, 2023, 45(03): 367-384.
[5] Xu X J, Liu B L, Pan D B, et al. Research and Application of Amphibious Bionic Robots [J]. Journal of Unmanned Undersea Systems, 2023, 31(01): 143-151.
[6] Sun C L, Xu X J, Tang Y J, et al. Experiment and Numerical Simulation on Drag Reduction and Speed Increase of Sectional Crawler Amphibious Vehicle [J]. Journal of National University of Defense Technology, 2022, 44(05): 201-208.
[7] Zhou R, You S X, Huang L, et al. Spatiotemporal Pattern Evolution and Driving Factors of the Globally Important Agricultural Heritage System Mulberry-Dyke and Fish-Pond [J]. Journal of Zhejiang University (Agriculture and Life Sciences), 2024, 50(02): 200-208.
[8] Bai X J, Shang J Z, Luo Z R, et al. Development and prospect of amphibious bionic robots [J]. Journal of Zhejiang University-Science A (Applied Physics & Engineering), 2022, 23(03): 157-188.

DOI: 10.54254/2755-2721/2026.BJ32898

[9] Zhao B X. Research on Wheel-Legged Amphibious Robot [D]. Harbin: Harbin Institute of Technology, 2021.
[10] Su Z S. Research Progress and Application of Amphibious Bionic Robots [J]. National Defense Technology, 2019, 40(04): 50-54.